

## Basic solution for three parallel non-symmetric permeable mode-III cracks in a functionally graded piezoelectric material plate

JUN LIANG

*Center for Composite Materials and Structures  
Harbin Institute of Technology  
P.O. Box 3010, No.2 Yikuang Street  
Harbin 150001, P.R.China  
e-mail: liangj@hit.edu.cn*

THE BEHAVIOR of three parallel permeable cracks with different lengths in a functionally graded piezoelectric material plane subjected to anti-plane shear stress loading was studied by the Schmidt method. The problem was formulated through the Fourier transform into three pairs of dual integral equations. To solve the dual integral equations, the jumps of displacements across the crack surfaces were directly expanded in a series of Jacobi polynomials. The results show that the stress and the electric displacement intensity factors at the crack tips depend on the lengths, spacing of the cracks and the material parameters. It is also revealed that the crack shielding effect is present in functionally graded piezoelectric materials.

**Key words:** functionally graded piezoelectric materials; multiple parallel non-symmetric cracks; crack shielding effect; couple field state; mechanics of solids.

Copyright © 2009 by IPPT PAN

### 1. Introduction

ELECTROMECHANICAL COUPLING EFFECTS in piezoelectric materials have been known for several years. However, only in recent years much interest has been generated because of their application to electronic devices, such as actuators and sensors. When subjected to mechanical and electrical loads in service, these piezoelectric materials can fail prematurely due to defects, e.g. cracks, holes, etc., arising during their manufacturing process. Therefore, it is of great importance to study the electro-elastic interaction and the fracture behavior of piezoelectric materials [1–6], especially when multiple cracks are involved.

On the other hand, the development of functionally graded materials (FGMs) has demonstrated that they have the potential to reduce the stress concentration and increase the fracture toughness. Consequently, the concept of FGMs can be extended to the piezoelectric materials to improve the reliability of piezoelectric materials and structures. Some application of functionally graded piezoelectric materials (FGPMs) have been made [7, 8]. The fracture problems of FGPMs

have been considered in [9–14]. LI and WENG [9] considered first the static anti-plane problem of a finite crack in a functionally graded piezoelectric material strip. Their results showed that the singular stress and electric displacements in functionally graded piezoelectric materials had the same forms as those in the homogeneous piezoelectric materials, but the magnitudes of the intensity factors depended significantly upon the gradient parameter of the functionally graded piezoelectric materials properties. The problems of electromechanical impact of a Mode-I impermeable crack in a functionally graded piezoelectric medium and a functionally graded piezoelectric strip were studied in [10, 11], respectively. Quite recently, more advanced crack problems in FGPMs have been published by other authors [15–18], considering Mode-I cracks with semi-permeable boundary conditions or applying numerical techniques. Because functionally graded piezoelectric materials are very brittle and cracked, functionally graded piezoelectric materials obviously contain multiple cracks with an extremely high crack density, the interaction between multiple cracks may significantly affect their fracture behavior. Knowledge of such a problem would allow us to fully exploit the merits of functionally graded piezoelectric materials. For these interesting multiple-crack problems in piezoelectric materials or in functionally graded piezoelectric materials, many studies have been conducted.

The problems of two parallel cracks or four parallel cracks in the piezoelectric materials were studied in [19–23]. The fracture problem of two parallel symmetric cracks in functionally graded piezoelectric/piezomagnetic materials was considered in [24], where only the symmetric fracture problems were considered. For the multiple cracks problems in piezoelectric materials or in functionally graded piezoelectric materials, some results were also given in the literature [25–28]. However, the number of cracks was infinite and the form of cracks was symmetric in [25–28], where only the symmetric fracture problems were considered. These fracture problems in piezoelectric materials or in functionally graded piezoelectric materials were solved by the representative crack unit method and the integral transform technique for periodic cracks in [25–28]. Other unknown variables of the dual integral equations were the dislocation density functions in [25–28]. Based upon these papers, a series of significant achievements for multiple cracks in piezoelectric materials or in functionally graded piezoelectric materials have been obtained [19–28]. However, relatively fewer studies have been conducted to deal with the interaction of multiple cracks in functionally graded piezoelectric materials. To our knowledge, the electro-elastic behavior of three arbitrary, parallel permeable cracks of different lengths in a functionally graded piezoelectric material plane subjected to anti-plane shear stress loading, has not been studied by using the Schmidt method [29], in which the properties of the materials varies exponentially with coordinates normal or parallel to the crack. It is with this in mind that we report the present work.

The interaction of three arbitrary, parallel permeable cracks with different lengths subjected to anti-plane shear loading in an infinite functionally graded piezoelectric material plate, was investigated using the Schmidt method [29] for two cases. In the first case it was assumed that the material properties varied exponentially in  $y$ -direction with the exponent  $\exp(\beta y)$ , and the other case assumed that the material properties varied exponentially in  $x$ -direction with the exponent  $\exp(\beta x)$ . Here, the direction of cracks is parallel to the  $x$ -axis.  $\beta$  is the functionally graded parameter.

### 2. Formulation of the problem

It is assumed that there are three arbitrary parallel permeable cracks 1, 2 and 3 of lengths  $2l_1$ ,  $2l_2$  and  $2l_3$ , parallel to each other in a functionally graded piezoelectric material plane as shown in Fig. 1. A Cartesian coordinate system  $(x, y)$  has the origin at the centre of crack 1, and  $x$ - and  $y$ -axis are parallel and perpendicular to the cracks, respectively, as shown in Fig. 1. For the convenience, we assume that  $h_1 = 0$  (it was not labeled in Fig. 1).  $h_2$  is the thickness of the layer 2 and is also the distance between the crack 1 and the crack 2.  $h_3$  is the thickness of the layer 2 and the layer 3, and it is also the distance between the crack 1 and the crack 3.  $d_1$ ,  $d_2$  and  $d_3$  are the  $x$ -coordinates of the centers of crack 1, crack 2 and crack 3, respectively. Here, the center of crack is the middle point between two crack tips. In the present paper, it is assumed that  $d_1 = 0$

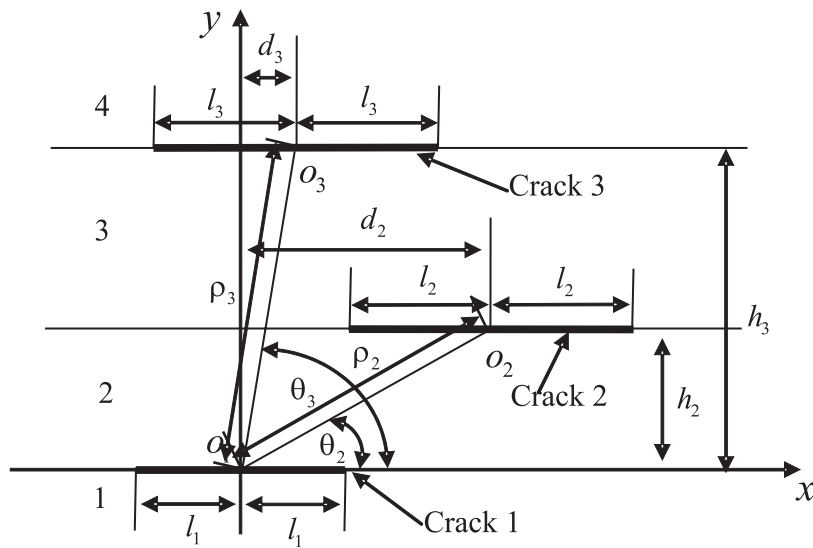


FIG. 1. Geometry and coordinate system for three parallel non-symmetric cracks.

(it was also not labeled in Fig. 1).  $\rho_2$  and  $\rho_3$  are the distances between the center of crack 1 and the centers of crack 2 and crack 3, respectively.  $\theta_1$  and  $\theta_2$  denote the location angles of the centers of crack 2 and crack 3 with respect to the center of crack 1 measured from the  $x$ -axis, as shown in Fig. 1.

It was assumed that a distributed anti-plane shear stress loading  $\tau_{yz}(x, 0) = -\tau_0$  (here  $\tau_0$  is the magnitude of the anti-plane shear stress loading) was directly applied on the cracks surfaces, which was equivalent to investigation of the perturbation fields for a remotely loaded cracked-body through the standard superposition technique in the fracture mechanics. Similar to SOH's [30] work, since no opening displacement exists for the present anti-plane shear problem, the crack surfaces can be assumed to be in perfect contact. Accordingly, permeable condition will be enforced in the present study, i.e., both the electric potential and the normal electric displacement are assumed to be continuous across the crack surfaces. Therefore the boundary conditions of the present problem were as follows:

$$(1) \quad \begin{cases} \tau_{yz}^{(j+1)}(x, h_j) = \tau_{yz}^{(j)}(x, h_j) = -\tau_0, \\ \phi^{(j+1)}(x, h_j) = \phi^{(j)}(x, h_j), \quad D_y^{(j+1)}(x, h_j) = D_y^{(j)}(x, h_j), \\ |x - d_j| \leq l_j \quad (j = 1, 2, 3), \end{cases}$$

$$(2) \quad \begin{cases} w^{(j+1)}(x, h_j) = w^{(j)}(x, h_j), \quad \tau_{yz}^{(j+1)}(x, h_j) = \tau_{yz}^{(j)}(x, h_j), \\ \phi^{(j+1)}(x, h_j) = \phi^{(j)}(x, h_j), \quad D_y^{(j+1)}(x, h_j) = D_y^{(j)}(x, h_j), \\ |x - d_j| > l_j \quad (j = 1, 2, 3), \end{cases}$$

$$(3) \quad w^{(j)}(x, y) = \phi^{(j)}(x, y) = 0 \quad \text{for } \sqrt{x^2 + y^2} \rightarrow \infty \quad (j = 1, 2, 3, 4),$$

where  $w^{(j)}(x, y)$  and  $\phi^{(j)}(x, y)$  ( $j = 1, 2, 3, 4$ ) are the mechanical displacement and the electric potential, respectively,  $\tau_{zk}^{(j)}(x, y)$  and  $D_k^{(j)}(x, y)$  ( $k = x, y$ ,  $j = 1, 2, 3, 4$ ) are the anti-plane shear stress field and in-plane electric displacement field, respectively, in which all quantities with superscript  $j$  ( $j = 1, 2, 3, 4$ ) correspond to the lower half-plane 1, the layer 2, the layer 3 and the upper half-plane 4, respectively, as shown in Fig. 1.

The constitutive equations for the Mode-III crack in transversely isotropic functionally graded piezoelectric materials can be expressed as follows:

$$(4) \quad \begin{cases} \tau_{kz}^{(j)} = c_{44}^* w_{,k}^{(j)} + e_{15}^* \phi_{,k}^{(j)}, \\ D_k^{(j)} = e_{15}^* w_{,k}^{(j)} - \varepsilon_{11}^* \phi_{,k}^{(j)}, \end{cases} \quad (k = x, y, j = 1, 2, 3, 4),$$

where  $c_{44}^*$ ,  $e_{15}^*$ ,  $\varepsilon_{11}^*$  are the shear modulus, piezoelectric coefficient and dielectric parameter of the functionally graded piezoelectric materials, respectively.

Crack problems in functionally graded materials do not appear to be analytically tractable for arbitrary variations of material properties. Usually, one tries to generate the forms of functionally graded materials for which the problem becomes tractable only. Similarly to the treatment of the crack problem for isotropic non-homogeneous materials used in [31, 32], we assume that the material properties are described for two cases as follows:

CASE I.

$$c_{44}^* = c_{44}e^{\beta y}, \quad e_{15}^* = e_{15}e^{\beta y}, \quad \varepsilon_{11}^* = \varepsilon_{11}e^{\beta y},$$

CASE II.

$$c_{44}^* = c_{44}e^{\beta x}, \quad e_{15}^* = e_{15}e^{\beta x}, \quad \varepsilon_{11}^* = \varepsilon_{11}e^{\beta x},$$

where  $\beta$  is the functionally graded parameter.  $c_{44}$ ,  $e_{15}$  and  $\varepsilon_{11}$  are the shear modulus, piezoelectric coefficient and dielectric parameter along the  $x$ -axis (Case I) or  $y$ -axis (Case II), respectively. The expressions of Eq. (5) are assumed for making the problem tractable without any loss of generality. In practice, the piecewise-exponential model can be used to approach the arbitrary distribution properties of FGMs, as discussed in [33].

The anti-plane governing equations of the functionally graded piezoelectric materials with vanishing body force and free charges can be written as follows:

CASE I.

$$(6-I) \quad \begin{cases} c_{44} \left( \nabla^2 w^{(j)} + \beta \frac{\partial w^{(j)}}{\partial y} \right) + e_{15} \left( \nabla^2 \phi^{(j)} + \beta \frac{\partial \phi^{(j)}}{\partial y} \right) = 0, \\ e_{15} \left( \nabla^2 w^{(j)} + \beta \frac{\partial w^{(j)}}{\partial y} \right) - \varepsilon_{11} \left( \nabla^2 \phi^{(j)} + \beta \frac{\partial \phi^{(j)}}{\partial y} \right) = 0, \end{cases} \quad (j = 1, 2, 3, 4).$$

CASE II.

$$(6-II) \quad \begin{cases} c_{44} \left( \nabla^2 w^{(j)} + \beta \frac{\partial w^{(j)}}{\partial x} \right) + e_{15} \left( \nabla^2 \phi^{(j)} + \beta \frac{\partial \phi^{(j)}}{\partial x} \right) = 0, \\ e_{15} \left( \nabla^2 w^{(j)} + \beta \frac{\partial w^{(j)}}{\partial x} \right) - \varepsilon_{11} \left( \nabla^2 \phi^{(j)} + \beta \frac{\partial \phi^{(j)}}{\partial x} \right) = 0, \end{cases} \quad (j = 1, 2, 3, 4)$$

where  $\nabla^2 = \partial^2/\partial x^2 + \partial^2/\partial y^2$  is the two-dimensional Laplace operator.

### 3. Solution

By applying Fourier transform to Eq. (6), the general expressions for the displacement components and electric potentials satisfying Eq. (3) can be written as follows:

CASE I.

$$(7-I) \quad \begin{cases} w^{(j)}(x, y) = \frac{1}{2\pi} \int_{-\infty}^{\infty} [A_j(s)e^{-\gamma_1(s)y} + B_j(s)e^{-\gamma_2(s)y}] e^{isx} ds, \\ \phi^{(j)}(x, y) = \frac{e_{15}}{\varepsilon_{11}} w^{(j)}(x, y) + \frac{1}{2\pi} \int_{-\infty}^{\infty} [C_j(s)e^{-\gamma_1(s)y} + D_j(s)e^{-\gamma_2(s)y}] e^{isx} ds \end{cases} \quad (y \in R_j, j = 1, 2, 3, 4).$$

CASE II.

$$(7-II) \quad \begin{cases} w^{(j)}(x, y) = \frac{1}{2\pi} \int_{-\infty}^{\infty} [A_j(s)e^{-\gamma(s)y} + B_j(s)e^{\gamma(s)y}] e^{isx} ds, \\ \phi^{(j)}(x, y) = \frac{e_{15}}{\varepsilon_{11}} w^{(j)}(x, y) + \frac{1}{2\pi} \int_{-\infty}^{\infty} [C_j(s)e^{-\gamma(s)y} + D_j(s)e^{\gamma(s)y}] e^{isx} ds \end{cases} \quad (y \in R_j, j = 1, 2, 3, 4).$$

where we assume for convenience that  $A_1(s) = C_1(s) = B_4(s) = D_4(s) = 0$ , and  $B_1(s), D_1(s), A_2(s), B_2(s), C_2(s), D_2(s), A_3(s), B_3(s), C_3(s), D_3(s), A_4(s), C_4(s)$  are unknown functions to be determined.  $R_1 = (-\infty, 0]$ ,  $R_2 = [0, h_2]$ ,  $R_3 = [h_2, h_3]$ ,  $R_4 = [h_3, +\infty)$ .  $\gamma_1(s) = (\beta + \sqrt{\beta^2 + 4s^2})/2$  and  $\gamma_2(s) = (\beta - \sqrt{\beta^2 + 4s^2})/2$  is valid for Case I,  $\gamma(s) = \sqrt{s^2 - is\beta}$  is valid for Case II, where  $i = \sqrt{-1}$ .

So from Eq. (4), we have:

CASE I.

$$(8-I) \quad \begin{cases} \tau_{yz}^{(j)}(x, y) = -\frac{e^{\beta y}}{2\pi} \int_{-\infty}^{\infty} \{ \gamma_1(s)[\mu_0 A_j(s) + e_{15} C_j(s)] e^{-\gamma_1(s)y} \\ \quad + \gamma_2(s)[\mu_0 B_j(s) + e_{15} D_j(s)] e^{-\gamma_2(s)y} \} e^{isx} ds, \\ D_y^{(j)}(x, y) = \frac{e^{\beta y}}{2\pi} \int_{-\infty}^{\infty} \varepsilon_{11} [\gamma_1(s) C_j(s) e^{-\gamma_1(s)y} + \gamma_2(s) D_j(s) e^{-\gamma_2(s)y}] e^{isx} ds \end{cases} \quad (y \in R_j, j = 1, 2, 3, 4).$$

CASE II.

$$(8-II) \quad \left\{ \begin{aligned} \tau_{yz}^{(j)}(x, y) &= -\frac{e^{\beta x}}{2\pi} \int_{-\infty}^{\infty} \gamma(s) \{ [\mu_0 A_j(s) + e_{15} C_j(s)] e^{-\gamma(s)y} \\ &\quad - [\mu_0 B_j(s) + e_{15} D_j(s)] e^{\gamma(s)y} \} e^{isx} ds, \\ D_y^{(j)}(x, y) &= \frac{e^{\beta x}}{2\pi} \int_{-\infty}^{\infty} \varepsilon_{11} \gamma(s) [C_j(s) e^{-\gamma(s)y} - D_j(s) e^{\gamma(s)y}] e^{isx} ds \end{aligned} \right. \quad (y \in R_j, \quad j = 1, 2, 3, 4)$$

where  $\mu_0 = c_{44} + \frac{e_{15}^2}{\varepsilon_{11}}$ .

To solve the problem, the jumps of displacements across the crack surfaces are defined as follows:

$$(9) \quad f_j(x) = w^{(j+1)}(x, h_j) - w^{(j)}(x, h_j) \quad (j = 1, 2, 3).$$

Substituting Eq. (7) into Eq. (9), and applying Eq. (8) and the boundary conditions Eq. (1) and Eq. (2), respectively, the following equations can be obtained using Fourier transform.

CASE I.

$$(10-I) \quad e^{-\gamma_2(s)h_j} [X_1] \begin{bmatrix} A_{j+1} \\ C_{j+1} \end{bmatrix} + e^{-\gamma_1(s)h_j} [X_1] \begin{bmatrix} B_{j+1} \\ D_{j+1} \end{bmatrix} - e^{-\gamma_2(s)h_j} [X_1] \begin{bmatrix} A_j \\ C_j \end{bmatrix} - e^{-\gamma_1(s)h_j} [X_1] \begin{bmatrix} B_j \\ D_j \end{bmatrix} = \begin{bmatrix} \bar{f}_j \\ 0 \end{bmatrix} \quad (j = 1, 2, 3),$$

$$(11-I) \quad \gamma_2(s) e^{-\gamma_2(s)h_j} [X_2] \begin{bmatrix} A_{j+1} \\ C_{j+1} \end{bmatrix} + \gamma_1(s) e^{-\gamma_1(s)h_j} [X_2] \begin{bmatrix} B_{j+1} \\ D_{j+1} \end{bmatrix} - \gamma_2(s) e^{-\gamma_2(s)h_j} [X_2] \begin{bmatrix} A_j \\ C_j \end{bmatrix} - \gamma_1(s) e^{-\gamma_1(s)h_j} [X_2] \begin{bmatrix} B_j \\ D_j \end{bmatrix} = \begin{bmatrix} 0 \\ 0 \end{bmatrix} \quad (j = 1, 2, 3).$$

CASE II.

$$(10-II) \quad e^{-\gamma(s)h_j} [X_1] \begin{bmatrix} A_{j+1} \\ C_{j+1} \end{bmatrix} + e^{\gamma(s)h_j} [X_1] \begin{bmatrix} B_{j+1} \\ D_{j+1} \end{bmatrix} - e^{-\gamma(s)h_j} [X_1] \begin{bmatrix} A_j \\ C_j \end{bmatrix} - e^{\gamma(s)h_j} [X_1] \begin{bmatrix} B_j \\ D_j \end{bmatrix} = \begin{bmatrix} \bar{f}_j \\ 0 \end{bmatrix} \quad (j = 1, 2, 3),$$

$$(11-II) \quad e^{-\gamma(s)h_j} [X_2] \begin{bmatrix} A_{j+1} \\ C_{j+1} \end{bmatrix} - e^{\gamma(s)h_j} [X_2] \begin{bmatrix} B_{j+1} \\ D_{j+1} \end{bmatrix} \\ - e^{-\gamma(s)h_j} [X_2] \begin{bmatrix} A_j \\ C_j \end{bmatrix} + e^{\gamma(s)h_j} [X_2] \begin{bmatrix} B_j \\ D_j \end{bmatrix} = \begin{bmatrix} 0 \\ 0 \end{bmatrix} \quad (j = 1, 2, 3)$$

where matrices

$$[X_1] = \begin{bmatrix} 1 & 0 \\ e_{15} & 1 \\ \varepsilon_{11} & \end{bmatrix}, \quad [X_2] = \begin{bmatrix} \mu_0 & e_{15} \\ 0 & -\varepsilon_{11} \end{bmatrix}$$

and symbol  $\bar{f}$  indicates the Fourier transform as follows:

$$(12) \quad \bar{f}(s) = \int_{-\infty}^{\infty} f(x) e^{-isx} dx.$$

Solving the twelve equations of Eqs. (10) and (11) with twelve unknown functions  $B_1(s)$ ,  $D_1(s)$ ,  $A_2(s)$ ,  $B_2(s)$ ,  $C_2(s)$ ,  $D_2(s)$ ,  $A_3(s)$ ,  $B_3(s)$ ,  $C_3(s)$ ,  $D_3(s)$ ,  $A_4(s)$ ,  $C_4(s)$  and applying the boundary conditions Eq. (1) and Eq. (2), we obtain:

CASE I.

$$(13-I) \quad \frac{c_{44}e^{\beta h_j}}{2\pi} \int_{-\infty}^{\infty} \sum_{k=1}^3 g_k^{(j)}(s) \bar{f}_k(s) e^{isx} ds = -\tau_0, \quad |x - d_j| \leq l_j \quad (j = 1, 2, 3),$$

$$(14-I) \quad \int_{-\infty}^{\infty} \bar{f}_j(s) e^{isx} ds = 0, \quad |x - d_j| > l_j \quad (j = 1, 2, 3),$$

where

$$g_k^{(k)}(s) = -\frac{s^2}{\sqrt{\beta^2 + 4s^2}} \quad (k = 1, 2, 3), \\ g_2^{(1)}(s) = -\frac{s^2 e^{\gamma_2(s)h_2}}{\sqrt{\beta^2 + 4s^2}}, \quad g_3^{(1)}(s) = -\frac{s^2 e^{\gamma_2(s)h_3}}{\sqrt{\beta^2 + 4s^2}}, \\ g_1^{(2)}(s) = -\frac{s^2 e^{-\gamma_1(s)h_2}}{\sqrt{\beta^2 + 4s^2}}, \quad g_3^{(2)}(s) = -\frac{s^2 e^{\gamma_2(s)(h_3-h_2)}}{\sqrt{\beta^2 + 4s^2}}, \\ g_1^{(3)}(s) = -\frac{s^2 e^{-\gamma_1(s)h_3}}{\sqrt{\beta^2 + 4s^2}}, \quad g_2^{(3)}(s) = -\frac{s^2 e^{-\gamma_1(s)(h_3-h_2)}}{\sqrt{\beta^2 + 4s^2}}.$$

Moreover,

$$\lim_{s \rightarrow +\infty} \frac{g_k^{(j)}(s)}{s} = - \lim_{s \rightarrow -\infty} \frac{g_k^{(j)}(s)}{s} = -\frac{1}{2} \quad (k=j) \quad \text{and} \quad \lim_{|s| \rightarrow \infty} \frac{g_k^{(j)}(s)}{s} = 0 \quad (k \neq j)$$

for Case I.

CASE II.

$$(13-II) \quad \frac{c_{44}e^{\beta x}}{2\pi} \int_{-\infty}^{\infty} \sum_{k=1}^3 g_k^{(j)}(s) \bar{f}_k(s) e^{isx} ds = -\tau_0, \quad |x - d_j| \leq l_j \quad (j = 1, 2, 3),$$

$$(14-II) \quad \int_{-\infty}^{\infty} \bar{f}_j(s) e^{isx} ds = 0, \quad |x - d_j| > l_j \quad (j = 1, 2, 3),$$

where

$$g_k^{(k)}(s) = -\frac{\gamma(s)}{2} \quad (k = 1, 2, 3),$$

$$g_2^{(1)}(s) = g_1^{(2)}(s) = -\frac{\gamma(s)e^{-\gamma(s)h_2}}{2},$$

$$g_3^{(1)}(s) = g_1^{(3)}(s) = -\frac{\gamma(s)e^{-\gamma(s)h_3}}{2},$$

$$g_3^{(2)}(s) = g_2^{(3)}(s) = -\frac{\gamma(s)e^{-\gamma(s)(h_3-h_1)}}{2}.$$

Moreover,

$$\lim_{s \rightarrow +\infty} \frac{g_k^{(j)}(s)}{s} = - \lim_{s \rightarrow -\infty} \frac{g_k^{(j)}(s)}{s} = -\frac{1}{2} \quad (k=j) \quad \text{and} \quad \lim_{|s| \rightarrow \infty} \frac{g_k^{(j)}(s)}{s} = 0 \quad (k \neq j)$$

for Case II.

The above dual integral equations (13) and (14) must be solved to determine the unknown functions  $f_1(x)$ ,  $f_2(x)$  and  $f_3(x)$ .

#### 4. Solution of the dual integral equation

The Schmidt method [29] was used to solve the dual integral equations (13) and (14). The jumps of displacements across the crack surfaces were represented by the following series:

$$(15) \quad f_j(x) = \begin{cases} \sum_{n=0}^{\infty} a_{jn} P_n^{(1/2,1/2)}\left(\frac{x - d_j}{l_j}\right) \left[1 - \frac{(x - d_j)^2}{l_j^2}\right]^{1/2}, & |x - d_j| \leq l_j, \\ 0, & |x - d_j| > l_j, \end{cases}$$

for  $(j = 1, 2, 3)$ , where  $a_{jn}$  are unknown coefficients to be determined and  $P_n^{(1/2, 1/2)}(x)$  is a Jacobi polynomial [34]. The Fourier transforms of Eq. (15) are [35] as follows:

$$(16) \quad \bar{f}_j(s) = \sum_{n=0}^{\infty} a_{jn} G_n \frac{1}{s} J_{n+1}(sl_j) e^{-isd_j},$$

$$G_n = 2\sqrt{\pi} (-1)^n i^n \frac{\Gamma(n+1+\frac{1}{2})}{n!}, \quad (j = 1, 2, 3),$$

where  $\Gamma(x)$  and  $J_n(x)$  are the gamma and Bessel functions of order  $n$ , respectively.

Substituting Eq. (16) into Eqs. (13) and (14), Equation (14) is automatically satisfied. Then Eq. (13) is reduced to the following forms after integration with respect to  $x$  for  $[d_j - l_j, x]$ , respectively:

CASE I.

$$(17-I) \quad \frac{c_{44} e^{\beta h_j}}{2\pi} \sum_{n=0}^{\infty} G_n \int_{-\infty}^{\infty} \frac{e^{isx} - e^{is(d_j-l_j)}}{is^2} \sum_{k=1}^3 a_{kn} g_k^{(j)}(s) J_{n+1}(sl_k) e^{-isd_k} ds$$

$$= -\tau_0(x - d_j + l_j), \quad |x - d_j| \leq l_j \quad (j = 1, 2, 3).$$

CASE II.

$$(17-II) \quad \frac{c_{44}}{2\pi} \sum_{n=0}^{\infty} G_n \int_{-\infty}^{\infty} \frac{e^{(is+\beta)x} - e^{(is+\beta)(d_j-l_j)}}{s(is+\beta)} \sum_{k=1}^3 a_{kn} g_k^{(j)}(s) J_{n+1}(sl_k) e^{-isd_k} ds$$

$$= -\tau_0(x - d_j + l_j), \quad |x - d_j| \leq l_j \quad (j = 1, 2, 3).$$

The semi-infinite integral in Eq. (17) can be modified as follows:

CASE I.

$$(18-I) \quad \int_{-\infty}^{\infty} \frac{1}{is^2} e^{-isd_j} g_j^{(j)}(s) J_{n+1}(sl_j) [e^{isx} - e^{is(d_j-l_j)}] ds$$

$$= - \begin{cases} \frac{-i}{n+1} \left\{ \cos \left[ (n+1) \sin^{-1} \left( \frac{x-d_j}{l_j} \right) \right] - (-1)^{(n+1)/2} \right\}, & n = 1, 3, 5, 7, \dots, \\ \frac{1}{n+1} \left\{ \sin \left[ (n+1) \sin^{-1} \left( \frac{x-d_j}{l_j} \right) \right] + (-1)^{n/2} \right\}, & n = 0, 2, 4, 6, \dots, \end{cases}$$

$$+ \int_0^{\infty} \frac{1}{is} e^{-isd_j} \left[ \frac{g_j^{(j)}(s)}{s} + \frac{1}{2} \right] J_{n+1}(sl_j) [e^{isx} - e^{is(d_j-l_j)}] ds$$

$$+ \int_{-\infty}^0 \frac{1}{is} e^{-isd_j} \left[ \frac{g_j^{(j)}(s)}{s} - \frac{1}{2} \right] J_{n+1}(sl_j) [e^{isx} - e^{is(d_j-l_j)}] ds \quad (j = 1, 2, 3).$$

CASE II.

$$\begin{aligned}
 (18-II) \quad & \int_{-\infty}^{\infty} \frac{1}{(is + \beta)s} e^{-isd_j} g_j^{(j)}(s) J_{n+1}(sl_j) [e^{(is+\beta)x} - e^{(is+\beta)(d_j-l_j)}] ds \\
 & = - \begin{cases} \frac{-i}{n+1} \left\{ \cos \left[ (n+1) \sin^{-1} \left( \frac{x-d_j}{l_j} \right) \right] e^{\beta x} \right. \\ \qquad \left. - (-1)^{(n+1)/2} e^{\beta(d_j-l_j)} \right\}, & n = 1, 3, 5, 7, \dots, \\ \frac{1}{n+1} \left\{ \sin \left[ (n+1) \sin^{-1} \left( \frac{x-d_j}{l_j} \right) \right] e^{\beta x} \right. \\ \qquad \left. + (-1)^{n/2} e^{\beta(d_j-l_j)} \right\}, & n = 0, 2, 4, 6, \dots, \end{cases} \\
 & \quad + \int_0^{\infty} \frac{1}{s} e^{-isd_j} \left[ \frac{g_j^{(j)}(s)}{is + \beta} + \frac{1}{2i} \right] J_{n+1}(sl_j) [e^{isx} - e^{is(d_j-l_j)}] ds \\
 & \quad + \int_{-\infty}^0 \frac{1}{s} e^{-isd_j} \left[ \frac{g_j^{(j)}(s)}{is + \beta} - \frac{1}{2i} \right] J_{n+1}(sl_j) [e^{isx} - e^{is(d_j-l_j)}] ds \quad (j = 1, 2, 3).
 \end{aligned}$$

It can be seen that the integrands of the semi-infinite integrals in the right-hand sides of Eq. (18) approach rapidly zero when  $s \rightarrow \infty$ . The semi-infinite integral in the left-hand side of Eq. (17) can be numerically evaluated easily. Thus Eq. (17) can now be solved for coefficients  $a_{jn}$  by the Schmidt method [29, 36, 37]. Details of the Schmidt method are presented in the Appendix.

### 5. Intensity factors

Once we determine the coefficients  $a_{jn}$ , we can obtain the entire perturbation stress field and the perturbation electric displacement near the crack tips. However, in fracture mechanics, it is of importance to determine the perturbation stress  $\tau_{yz}$  and the perturbation electric displacement  $D_y$  in the vicinity of the crack tips. In the present study,  $\tau_{yz}^{(1)}$ ,  $\tau_{yz}^{(2)}$ ,  $\tau_{yz}^{(3)}$ ,  $D_y^{(1)}$ ,  $D_y^{(2)}$  and  $D_y^{(3)}$  along the crack line can be expressed, respectively, as follows:

CASE I.

$$\begin{aligned}
 (19-I) \quad & \tau_{yz}^{(j)}(x, h_j) = \tau_{yz}^{(j+1)}(x, h_j) \\
 & = \frac{c_{44} e^{\beta h_j}}{2\pi} \sum_{n=0}^{\infty} G_n \int_{-\infty}^{\infty} \frac{1}{s} \left[ a_{1n} g_1^{(j)}(s) J_{n+1}(sl_1) + a_{2n} g_2^{(j)}(s) J_{n+1}(sl_2) e^{-isd_2} \right. \\
 & \qquad \left. + a_{3n} g_3^{(j)}(s) J_{n+1}(sl_3) e^{-isd_3} \right] e^{isx} ds \quad (j = 1, 2, 3),
 \end{aligned}$$

$$\begin{aligned}
(20-I) \quad D_y^{(j)}(x, h_j) &= D_y^{(j+1)}(x, h_j) \\
&= \frac{e_{15}e^{\beta h_j}}{2\pi} \sum_{n=0}^{\infty} G_n \int_{-\infty}^{\infty} \frac{1}{s} \left[ a_{1n}g_1^{(j)}(s)J_{n+1}(sl_1) + a_{2n}g_2^{(j)}(s)J_{n+1}(sl_2)e^{-isd_2} \right. \\
&\quad \left. + a_{3n}g_3^{(j)}(s)J_{n+1}(sl_3)e^{-isd_3} \right] e^{isx} ds \quad (j = 1, 2, 3).
\end{aligned}$$

CASE II.

$$\begin{aligned}
(19-II) \quad \tau_{yz}^{(j)}(x, h_j) &= \tau_{yz}^{(j+1)}(x, h_j) \\
&= \frac{c_{44}e^{\beta x}}{2\pi} \sum_{n=0}^{\infty} G_n \int_{-\infty}^{\infty} \frac{1}{s} \left[ a_{1n}g_1^{(j)}(s)J_{n+1}(sl_1) + a_{2n}g_2^{(j)}(s)J_{n+1}(sl_2)e^{-isd_2} \right. \\
&\quad \left. + a_{3n}g_3^{(j)}(s)J_{n+1}(sl_3)e^{-isd_3} \right] e^{isx} ds \quad (j = 1, 2, 3),
\end{aligned}$$

$$\begin{aligned}
(20-II) \quad D_y^{(j)}(x, h_j) &= D_y^{(j+1)}(x, h_j) \\
&= \frac{e_{15}e^{\beta x}}{2\pi} \sum_{n=0}^{\infty} G_n \int_{-\infty}^{\infty} \frac{1}{s} \left[ a_{1n}g_1^{(j)}(s)J_{n+1}(sl_1) + a_{2n}g_2^{(j)}(s)J_{n+1}(sl_2)e^{-isd_2} \right. \\
&\quad \left. + a_{3n}g_3^{(j)}(s)J_{n+1}(sl_3)e^{-isd_3} \right] e^{isx} ds \quad (j = 1, 2, 3).
\end{aligned}$$

The following relationships [34] are used later in the solving processes:

$$\int_0^{\infty} J_n(sa) \cos(bs) ds = \begin{cases} \frac{\cos[n \sin^{-1}(b/a)]}{\sqrt{a^2 - b^2}}, & a > b, \\ -\frac{a^n \sin(n\pi/2)}{\sqrt{b^2 - a^2}[b + \sqrt{b^2 - a^2}]^n}, & b > a, \end{cases}$$

$$\int_0^{\infty} J_n(sa) \sin(bs) ds = \begin{cases} \frac{\sin[n \sin^{-1}(b/a)]}{\sqrt{a^2 - b^2}}, & a > b, \\ \frac{a^n \cos(n\pi/2)}{\sqrt{b^2 - a^2}[b + \sqrt{b^2 - a^2}]^n}, & b > a. \end{cases}$$

CASE I. From Eqs. (19-I), (20-I) and (21-I), the singular parts of stress and electric displacement fields near the right-hand tip of the crack  $j$  ( $j = 1, 2, 3$ ) can be expressed, respectively, as follows ( $d_j + l_j < x$ ):

$$(22-I) \left\{ \begin{aligned} \tau_{jyz}^R &= -\frac{c_{44}e^{\beta h_j}}{4\pi} \sum_{n=0}^{\infty} a_{jn} G_n \left[ \int_0^{\infty} J_{n+1}(sl_j) e^{is(x-d_j)} ds \right. \\ &\quad \left. - \int_{-\infty}^0 J_{n+1}(sl_j) e^{is(x-d_j)} ds \right] = -\frac{c_{44}e^{\beta h_j}}{4\pi} \sum_{n=0}^{\infty} a_{jn} G_n Q_{jn}(x), \\ D_{jy}^R &= -\frac{e_{15}e^{\beta h_j}}{4\pi} \sum_{n=0}^{\infty} a_{jn} G_n \left[ \int_0^{\infty} J_{n+1}(sl_j) e^{is(x-d_j)} ds \right. \\ &\quad \left. - \int_{-\infty}^0 J_{n+1}(sl_j) e^{is(x-d_j)} ds \right] = -\frac{e_{15}e^{\beta h_j}}{4\pi} \sum_{n=0}^{\infty} a_{jn} G_n Q_{jn}(x), \end{aligned} \right.$$

where

$$Q_{jn}(x) = \frac{2(-1)^{(n+2)/2} l_j^{n+1}}{\sqrt{(x-d_j)^2 - l_j^2} [x-d_j + \sqrt{(x-d_j)^2 - l_j^2}]^{n+1}},$$

and the singular parts of stress and electric displacement fields near the left-hand tip of the crack  $j$  ( $j = 1, 2, 3$ ) can be expressed, respectively, as follows ( $x < d_j - l_j$ ):

$$(23-I) \left\{ \begin{aligned} \tau_{jyz}^L &= -\frac{c_{44}e^{\beta h_j}}{4\pi} \sum_{n=0}^{\infty} a_{jn} G_n \left[ \int_0^{\infty} J_{n+1}(sl_j) e^{is(x-d_j)} ds \right. \\ &\quad \left. - \int_{-\infty}^0 J_{n+1}(sl_j) e^{is(x-d_j)} ds \right] = -\frac{c_{44}e^{\beta h_j}}{4\pi} \sum_{n=0}^{\infty} a_{jn} G_n Q_{jn}^*(x), \\ D_{jy}^L &= -\frac{e_{15}e^{\beta h_j}}{4\pi} \sum_{n=0}^{\infty} a_{jn} G_n \left[ \int_0^{\infty} J_{n+1}(sl_j) e^{is(x-d_j)} ds \right. \\ &\quad \left. - \int_{-\infty}^0 J_{n+1}(sl_j) e^{is(x-d_j)} ds \right] = -\frac{e_{15}e^{\beta h_j}}{4\pi} \sum_{n=0}^{\infty} a_{jn} G_n Q_{jn}^*(x), \end{aligned} \right.$$

where

$$Q_{jn}^*(x) = \frac{2(-1)^{(3n+2)/2} l_j^{n+1}}{\sqrt{(x-d_j)^2 - l_j^2} [|x-d_j| + \sqrt{(x-d_j)^2 - l_j^2}]^{n+1}}.$$

CASE II. From Eqs. (19-II), (20-II) and (21-II), the singular parts of stress and electric displacement fields near the right-hand tip of the crack  $j$  ( $j = 1, 2, 3$ )

can be expressed, respectively, as follows ( $d_j + l_j < x$ ):

$$(22-II) \quad \left\{ \begin{array}{l} \tau_{jyz}^R = -\frac{c_{44}e^{\beta x}}{4\pi} \sum_{n=0}^{\infty} a_{jn} G_n \left[ \int_0^{\infty} J_{n+1}(sl_j) e^{is(x-d_j)} ds \right. \\ \left. - \int_{-\infty}^0 J_{n+1}(sl_j) e^{is(x-d_j)} ds \right] = -\frac{c_{44}e^{\beta x}}{4\pi} \sum_{n=0}^{\infty} a_{jn} G_n Q_{jn}(x), \\ D_{jy}^R = -\frac{e_{15}e^{\beta x}}{4\pi} \sum_{n=0}^{\infty} a_{jn} G_n \left[ \int_0^{\infty} J_{n+1}(sl_j) e^{is(x-d_j)} ds \right. \\ \left. - \int_{-\infty}^0 J_{n+1}(sl_j) e^{is(x-d_j)} ds \right] = -\frac{e_{15}e^{\beta x}}{4\pi} \sum_{n=0}^{\infty} a_{jn} G_n Q_{jn}(x), \end{array} \right.$$

and the singular parts of stress and electric displacement fields near the left-hand tip of the crack  $j$  ( $j = 1, 2, 3$ ) can be expressed, respectively, as follows ( $x < d_j - l_j$ ):

$$(23-II) \quad \left\{ \begin{array}{l} \tau_{jyz}^L = -\frac{c_{44}e^{\beta x}}{4\pi} \sum_{n=0}^{\infty} a_{jn} G_n \left[ \int_0^{\infty} J_{n+1}(sl_j) e^{is(x-d_j)} ds \right. \\ \left. - \int_{-\infty}^0 J_{n+1}(sl_j) e^{is(x-d_j)} ds \right] = -\frac{c_{44}e^{\beta x}}{4\pi} \sum_{n=0}^{\infty} a_{jn} G_n Q_{jn}^*(x), \\ D_{jy}^L = -\frac{e_{15}e^{\beta x}}{4\pi} \sum_{n=0}^{\infty} a_{jn} G_n \left[ \int_0^{\infty} J_{n+1}(sl_j) e^{is(x-d_j)} ds \right. \\ \left. - \int_{-\infty}^0 J_{n+1}(sl_j) e^{is(x-d_j)} ds \right] = -\frac{e_{15}e^{\beta x}}{4\pi} \sum_{n=0}^{\infty} a_{jn} G_n Q_{jn}^*(x). \end{array} \right.$$

CASE I. The stress intensity factor  $K_j^R$  and the electric displacement intensity factor  $K_{jD}^R$  at the right-hand tip of the crack  $j$  ( $j = 1, 2, 3$ ) can be obtained as follows:

$$(24-I) \quad \begin{aligned} K_j^R &= \lim_{x \rightarrow (d_j + l_j)^+} \sqrt{2(x - d_j - l_j)} \cdot \tau_{jyz}^R \\ &= \frac{c_{44}e^{\beta l_j}}{\sqrt{\pi l_j}} \sum_{n=0}^{\infty} a_{jn} \frac{\Gamma(n + 1 + \frac{1}{2})}{n!}, \end{aligned}$$

$$\begin{aligned}
(25-I) \quad K_{jD}^R &= \lim_{x \rightarrow (d_j+l_j)^+} \sqrt{2(x-d_j-l_j)} \cdot D_{jy}^R \\
&= \frac{e_{15}e^{\beta h_j}}{\sqrt{\pi l_j}} \sum_{n=0}^{\infty} a_{jn} \frac{\Gamma(n+1+\frac{1}{2})}{n!} = \frac{e_{15}}{c_{44}} K_j^R.
\end{aligned}$$

Similarly, the stress intensity factor  $K_j^L$  and the electric displacement intensity factor  $K_{jD}^L$  at the left tip of the crack  $j$  ( $j = 1, 2, 3$ ) are expressed as follows:

$$\begin{aligned}
(26-I) \quad K_j^L &= \lim_{x \rightarrow (d_j-l_j)^-} \sqrt{2|x-d_j+l_j|} \cdot \tau_{jyz}^L \\
&= \frac{c_{44}e^{\beta h_j}}{\sqrt{\pi l_j}} \sum_{n=0}^{\infty} (-1)^n a_{jn} \frac{\Gamma(n+1+\frac{1}{2})}{n!},
\end{aligned}$$

$$\begin{aligned}
(27-I) \quad K_{jD}^L &= \lim_{x \rightarrow (d_j-l_j)^-} \sqrt{2|x-d_j+l_j|} \cdot D_{jy}^L \\
&= \frac{e_{15}e^{\beta h_j}}{\sqrt{\pi l_j}} \sum_{n=0}^{\infty} (-1)^n a_{jn} \frac{\Gamma(n+1+\frac{1}{2})}{n!} = \frac{e_{15}}{c_{44}} K_j^L.
\end{aligned}$$

CASE II. The stress intensity factor  $K_j^R$  and the electric displacement intensity factor  $K_{jD}^R$  at the right-hand tip of the crack  $j$  ( $j = 1, 2, 3$ ) can be given as follows:

$$\begin{aligned}
(24-II) \quad K_j^R &= \lim_{x \rightarrow (d_j+l_j)^+} \sqrt{2(x-d_j-l_j)} \cdot \tau_{jyz}^R \\
&= \frac{c_{44}e^{\beta(d_j+l_j)}}{\sqrt{\pi l_j}} \sum_{n=0}^{\infty} a_{jn} \frac{\Gamma(n+1+\frac{1}{2})}{n!},
\end{aligned}$$

$$\begin{aligned}
(25-II) \quad K_{jD}^R &= \lim_{x \rightarrow (d_j+l_j)^+} \sqrt{2(x-d_j-l_j)} \cdot D_{jy}^R \\
&= \frac{e_{15}e^{\beta(d_j+l_j)}}{\sqrt{\pi l_j}} \sum_{n=0}^{\infty} a_{jn} \frac{\Gamma(n+1+\frac{1}{2})}{n!} = \frac{e_{15}}{c_{44}} K_j^R.
\end{aligned}$$

Similarly, the stress intensity factor  $K_j^L$  and the electric displacement intensity factor  $K_{jD}^L$  at the left tip of the crack  $j$  ( $j = 1, 2, 3$ ) are represented as follows:

$$\begin{aligned}
(26-II) \quad K_j^L &= \lim_{x \rightarrow (d_j-l_j)^-} \sqrt{2|x-d_j+l_j|} \cdot \tau_{jyz}^L \\
&= \frac{c_{44}e^{\beta(d_j-l_j)}}{\sqrt{\pi l_j}} \sum_{n=0}^{\infty} (-1)^n a_{jn} \frac{\Gamma(n+1+\frac{1}{2})}{n!},
\end{aligned}$$

$$\begin{aligned}
(27-II) \quad K_{jD}^L &= \lim_{x \rightarrow (d_j - l_j)^-} \sqrt{2|x - d_j + l_j|} \cdot D_{jy}^L \\
&= \frac{e_{15} e^{\beta(d_j - l_j)}}{\sqrt{\pi l_j}} \sum_{n=0}^{\infty} (-1)^n a_{jn} \frac{\Gamma(n + 1 + \frac{1}{2})}{n!} = \frac{e_{15}}{c_{44}} K_j^L.
\end{aligned}$$

## 6. Numerical calculations and conclusions

From the papers [29, 36, 37], it is known that the magnitudes of the unknown coefficients  $a_{jn}$  ( $j = 1, 2, 3$ ) in the infinite series (17) decrease very quickly with the increase of the number of terms  $n$ . The behavior of the sum of the series remains steady with the increase of the number of terms in the infinite series (17). The precision can be achieved satisfactorily if the first ten terms of the infinite series (17) are adopted. For brevity, these expressions are not given in the present paper. The stress intensity factors  $K$  and the electric displacement intensity factors  $K_D$  are calculated numerically. In all computations that follow, the piezoelectric material constants are assumed to be  $c_{44} = 2.56 \times 10^{10}$  (N/m<sup>2</sup>),  $e_{15} = 13.44$  (C/m<sup>2</sup>) and  $\varepsilon_{11} = 60.0 \times 10^{-10}$  (C/Vm). The calculated stress and electric displacement intensity factors at the crack tips are plotted in Figs. 2 to 23, respectively. We discuss the results and draw our conclusions as follows:

(i) In the present paper, the basic solution for three arbitrary parallel permeable Mode-III cracks with different lengths in functionally graded piezoelectric materials was obtained by the Schmidt method, which is quite different from the previous work on multiple cracks [25–28]. In [25–28], although the number of cracks is infinite, the cracks are arranged in a regular pattern, such that the fracture problems can be solved by the representative crack unit method and the integral transform technique for the periodic cracks. The unknown variables of dual integral equations are the dislocation density functions in [25–28]. Different from all these papers, in the present work, the crack distribution is non-symmetric, the number of cracks is finite and the unknown variables of dual integral equations are the jumps of displacements across the crack surfaces. The number of dual integral equations is assumed to be six in the present paper. Other the properties of materials of the present paper are different from the ones of the previous work [25, 27, 28]. To solve the dual integral equations, the jumps of displacements across the crack surfaces were directly expanded into a series of Jacobi polynomials, and the Schmidt method was used for numerical calculations in the present paper. This is the major difference between the present paper and the similar papers available in the literature [25–28].

(ii) The electro-elastic coupling effects can be obtained as shown in Eqs. (24)–(27). The results of the electric displacement intensity factors can be directly obtained from the results of stress intensity factors through these equations. As shown in Eqs. (17) and (24)–(27), it can be obtained that the electric

displacement intensity factors of cracks depend on the material constants  $c_{44}$  and  $e_{15}$ , the crack length, the geometric position of cracks and the distance between three parallel cracks. However, the stress intensity factors of cracks depend only on the crack length, the geometric position of cracks and the distance between three parallel cracks. The stress intensity factors of cracks are independent of material constants  $c_{44}$  and  $e_{15}$  as shown in Eqs. (17), (24) and Eq. (26).

(iii) In order to present the solving process and the calculation program, the results of three symmetric parallel cracks in a homogeneous material plane were calculated first and shown in Fig. 2. In this case, we obtain  $K_1^L = K_1^R = K_3^L = K_3^R = K_1 = K_3$  and  $K_2^L = K_2^R = K_2$ , what is consistent with the theoretical solution. The stress intensity factors of cracks increase with the increase of the crack spacing, then they tend to a constant 1 which equal to the intensity factor of a single crack in an infinite, functionally graded material plane. This phenomenon is called the crack shielding effect, as discussed in [38], which also proves that the solving process is correct.

CASE I. (iv) The stress intensity factors of cracks increase with the increase of the crack spacing and then they tend to constants as shown in Fig. 3. Here,  $K_1^L = K_1^R = K_1$ ,  $K_2^L = K_2^R = K_2$  and  $K_3^L = K_3^R = K_3$ , with the parameters chosen in the calculation. In this case, the stress intensity factors of crack 1 are less than the ones of crack 2 at the beginning, and they all tend to a constant 1 with the increase of  $h_2/l_1$  (or  $h_3/l_1$ ), with the parameters chosen in the calculation. This may be caused by the shielding effects of the parallel cracks. In this case, increasing of the distance between the two parallel cracks plays a similar role as decreasing of the length of crack for the present problem. For the electric displacement intensity factors, they have the same changing tendency as the stress intensity factors shown in Fig. 4 ( $K_{1D}^L =$

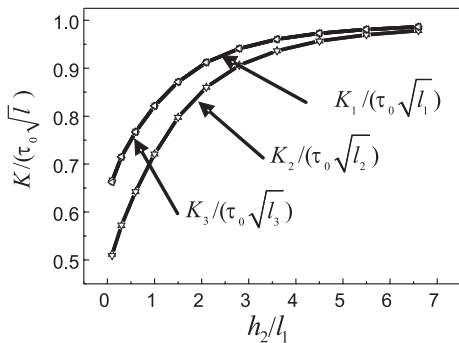


FIG. 2. Stress intensity factors of cracks versus  $h_2/l_1$  for  $\beta l_1 = 0.0$ ,  $l_2/l_1 = l_3/l_1 = 1.0$ ,  $d_2/l_1 = d_3/l_1 = 0.0$  and  $2h_2/l_1 = h_3/l_1$ .

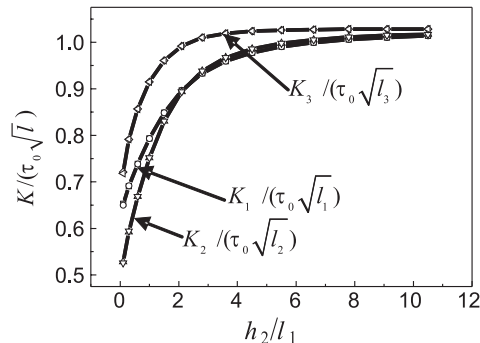


FIG. 3. Stress intensity factors at the tips of cracks versus  $h_2/l_1$  for  $\beta l_1 = -0.5$ ,  $l_2/l_1 = l_3/l_1 = 1.0$ ,  $d_2/l_1 = d_3/l_1 = 0.0$  and  $2h_2/l_1 = h_3/l_1$  (Case I).

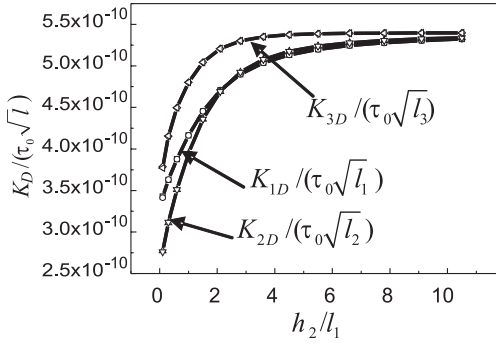


FIG. 4. Electric displacement intensity factors at the tips of cracks versus  $h_2/l_1$  for  $\beta l_1 = -0.5$ ,  $l_2/l_1 = l_3/l_1 = 1.0$ ,  $d_2/l_1 = d_3/l_1 = 0.0$  and  $2h_2/l_1 = h_3/l_1$  (Case I).

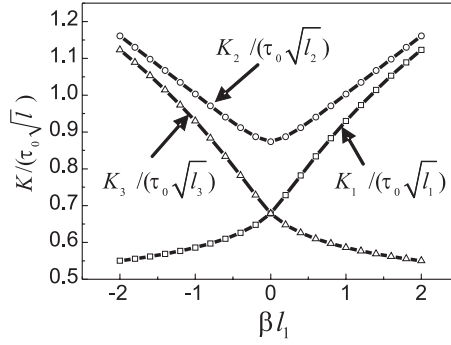


FIG. 5. Stress intensity factors at the tips of cracks versus  $\beta l_1$  for  $l_1 = 1.0$ ,  $l_2/l_1 = 1.5$ ,  $l_3/l_1 = 0.0$ ,  $d_2/l_1 = 0.0$ ,  $d_2/l_1 = 0.0$ ,  $d_3/l_1 = 0.0$ ,  $h_2/l_1 = 1.0$  and  $h_3/l_1 = 2.0$  (Case I).

$K_{1D}^R = K_{1D}$ ,  $K_{2D}^L = K_{2D}^R = K_{2D}$  and  $K_{3D}^L = K_{3D}^R = K_{3D}$  with the parameters chosen in the calculation). This can be obviously obtained from Eqs. (24)–(27). Hence, we only need to discuss the behavior of the stress intensity factors thereafter. However, the amplitude values of the electric displacement intensity factors and the stress intensity factors are different. The amplitude values of the electric displacement intensity factors are extremely small, as shown in Fig. 4.

(v) The geometric form of cracks is symmetrical about the  $y$ -axis and the line of crack 2 in this case, so the stress intensity factors at the left-hand tips are equal to those at the right-hand tips for every crack with the parameters chosen in the calculation, as shown in Fig. 5. Here,  $K_1^L = K_1^R = K_1$ ,  $K_2^L = K_2^R = K_2$  and  $K_3^L = K_3^R = K_3$ . The stress intensity factors of crack 1 increase with the increase of  $\beta l_1$ , but the stress intensity factors of crack 3 decrease with increasing  $\beta l_1$ . The stress intensity factors of crack 2 decrease with increasing  $\beta l_1$  for  $\beta l_1 < 0$ . However, the stress intensity factors of crack 2 increase with the increasing  $\beta l_1$  for  $\beta l_1 > 0$ , as shown in Fig. 5. It can be also obtained that  $K_1(\beta l_1) = K_1(-\beta l_1)$ ,  $K_2(\beta l_1) = K_2(-\beta l_1)$  and  $K_3(\beta l_1) = K_3(-\beta l_1)$  for this symmetric case, with the parameters chosen in the calculation. This is also consistent with the practical results. For  $\beta l_1 < 0$ , the stress intensity factors of crack 3 are larger than the ones of crack 1. However, the stress intensity factors of crack 1 are larger than the ones of crack 3 for  $\beta l_1 > 0$ . It means that the stress intensity factors of a crack on the stiffer side of the medium are always smaller than the ones of the crack located on the less stiff side, when the lengths of cracks are the same and the direction of the material properties variation is perpendicular to the cracks. However, the stress intensity factors of crack 2 are always larger than the ones of crack 1 or crack 3, because the length of crack 2 is larger than the ones of crack 1 or crack 3, with the parameters chosen in the calculation.

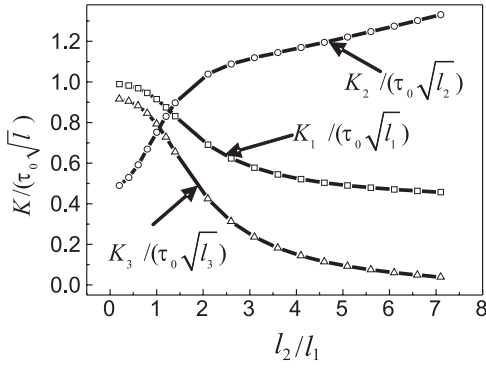


FIG. 6. Stress intensity factors at the tips of cracks versus  $l_2/l_1$  for  $\beta l_1 = 0.5$ ,  $l_3/l_1 = 1.0$ ,  $d_2/l_1 = d_3/l_1 = 0.0$ ,  $h_2/l_1 = 1.0$  and  $h_3/l_1 = 2.0$  (Case I).

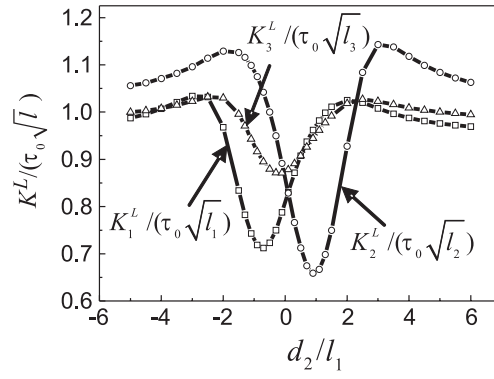


FIG. 7. Stress intensity factors at the left tips of cracks versus  $d_2/l_1$  for  $\beta l_1 = -0.5$ ,  $l_2/l_1 = l_3/l_1 = 1.0$ ,  $d_3/l_1 = 0.5$ ,  $h_2/l_1 = 1.0$  and  $h_3/l_1 = 2.0$  (Case I).

(vi) As shown in Fig. 6, the stress intensity factors of cracks 1 and crack 3 decrease with the increase of  $l_2/l_1$  with the parameters chosen in the calculation. In this case, we obtain  $K_1^L = K_1^R = K_1$ ,  $K_2^L = K_2^R = K_2$  and  $K_3^L = K_3^R = K_3$ . This phenomenon is also called the crack shielding effect as discussed in [38]. In this case, the increase of the crack length plays the same role as the decrease of spacing between two adjacent parallel cracks. However, the stress intensity factors of crack 2 increase with the increase of  $l_2/l_1$ . This means that the resistance expanding the ability of crack 2 decreases with the increase of its length  $l_2$ .

(vii) For all the three cracks, the stress intensity factors will tend to constants for  $|d_2/l_1| > 4.5$  as shown in Fig. 7 and Fig. 8. This means that the effects of  $d_2/l_1$

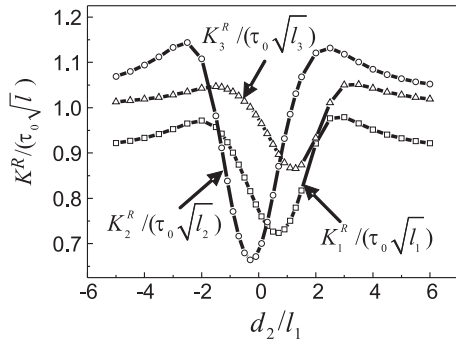


FIG. 8. Stress intensity factors at the right tips of cracks versus  $d_2/l_1$  for  $\beta l_1 = -0.5$ ,  $l_2/l_1 = l_3/l_1 = 1.0$ ,  $d_3/l_1 = 0.5$ ,  $h_2/l_1 = 1.0$  and  $h_3/l_1 = 2.0$  (Case I).

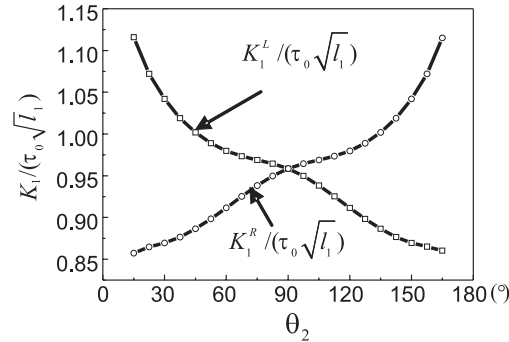


FIG. 9. Stress intensity factors at the tips of crack 1 versus  $\theta_2$  for  $\beta l_1 = 0.5$ ,  $l_2/l_1 = l_3/l_1 = 1.0$ ,  $\rho_2/l_1 = 1.5$ ,  $\rho_3/l_1 = 2.0$  and  $\theta_3 = 90^\circ$  (Case I).

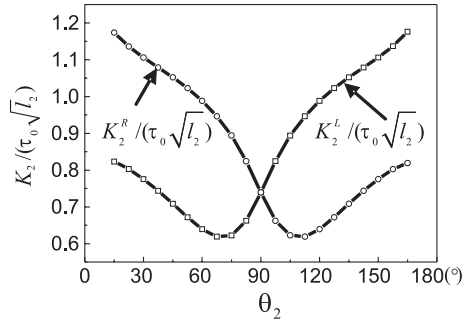


FIG. 10. Stress intensity factors at the tips of crack 2 versus  $\theta_2$  for  $\beta l_1 = 0.5$ ,  $l_2/l_1 = l_3/l_1 = 1.0$ ,  $\rho_2/l_1 = 1.5$ ,  $\rho_3/l_1 = 2.0$  and  $\theta_3 = 90^\circ$  (Case I).

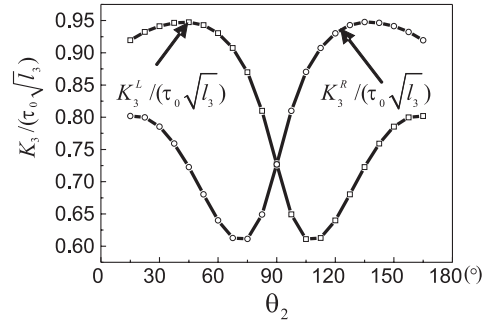


FIG. 11. Stress intensity factors at the tips of crack 3 versus  $\theta_2$  for  $\beta l_1 = 0.5$ ,  $l_2/l_1 = l_3/l_1 = 1.0$ ,  $\rho_2/l_1 = 1.5$ ,  $\rho_3/l_1 = 2.0$  and  $\theta_3 = 90^\circ$  (Case I).

on stress intensity factors will become mild for  $|d_2/l_1| > 4.5$ . However, the stress intensity factors of cracks oscillate with the variation of  $d_2/l_1$  for  $|d_2/l_1| < 4.0$ . The stress intensity factors will reach different minimum and maximum peak values at different positions of cracks. So it can be concluded that the crack positions also play a very important role in the stress intensity factors of the three parallel cracks for  $|d_2/l_1| < 4.0$ .

(viii) As shown in Figs. 9–11, the plots of the stress intensity factors at both crack tips of each crack are symmetric about the axis  $\theta_2 = 90^\circ$ , i.e.  $K_1^L(90^\circ \pm \theta) = K_1^R(90^\circ \mp \theta)$ ,  $K_2^L(90^\circ \pm \theta) = K_2^R(90^\circ \mp \theta)$  and  $K_3^L(90^\circ \pm \theta) = K_3^R(90^\circ \mp \theta)$  with the parameters chosen in the calculation. The stress intensity factor at the right tip of crack 1 increases with the increase of  $\theta_2$ . However, the stress intensity factor at the left tip of crack 1 decreases with the increase of  $\theta_2$ , as shown in Fig. 9. The stress intensity factors at the left tip and at the right tip of crack 2 decrease with the increase of  $\theta_2$ , to reach the minimum values at  $\theta_1 = 82.5^\circ$  and  $\theta_1 = 97.5^\circ$ , respectively, then they increase as shown in Fig. 10. The changing tendencies of stress intensity factors at the tips of crack 3 are more complex, as shown in Fig. 11. They have both the maximum values and the minimum values. These phenomena were also caused by the competition between the crack shielding effect and the interaction of parallel cracks. Two factors affect the results of the stress intensity factors of cracks: the first one is the vertical spacing  $h_3/l_1 - h_2/l_1$  between crack 2 and crack 3, and the second one is the horizontal distance between the centers of crack 2 and crack 3. Again, Figs. 9–11 are symmetric about the line of  $\theta_2 = 90^\circ$ .

CASE II. (ix) The crack shielding effects are also observed as discussed in [38] for the Case II, i.e., the stress intensity factors of cracks start to grow with the increase of the crack spacing, then they tend to constants as shown

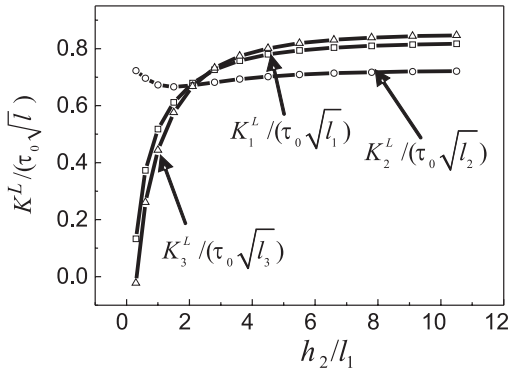


FIG. 12. Stress intensity factors at the left tips of cracks versus  $h_2/l_1$  for  $\beta l = 0.5$ ,  $l_2/l_1 = 1.5$ ,  $l_3/l_1 = 1.0$ ,  $d_2/l_1 = 0.0$ ,  $d_3/l_1 = 0.5$  and  $2h_2/l_1 = h_3/l_1$  (Case II).

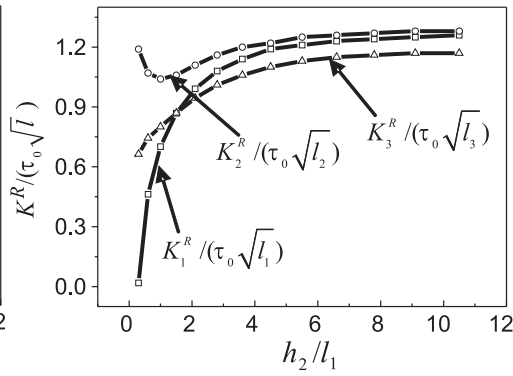


FIG. 13. Stress intensity factors at the right tips of cracks versus  $h_2/l_1$  for  $\beta l = 0.5$ ,  $l_2/l_1 = 1.5$ ,  $l_3/l_1 = 1.0$ ,  $d_2/l_1 = 0.0$ ,  $d_3/l_1 = 0.5$  and  $2h_2/l_1 = h_3/l_1$  (Case II).

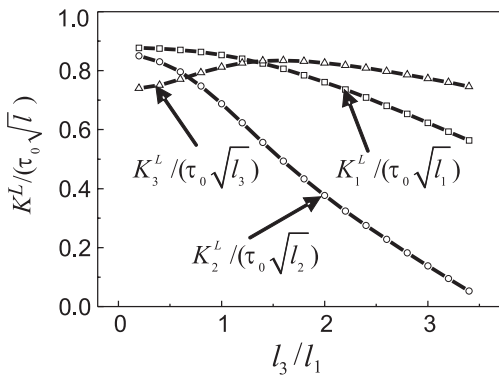


FIG. 14. Stress intensity factors at the left tips of cracks versus  $l_3$  for  $\beta = 0.2$ ,  $l_1 = 1.0$ ,  $l_2 = 0.8$ ,  $d_2 = 0.0$ ,  $d_3 = 0.0$ ,  $h_2 = 2.0$  and  $h_3 = 3.0$  (Case II).

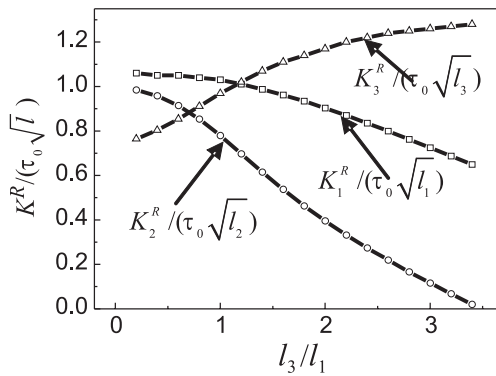


FIG. 15. Stress intensity factors at the right tips of cracks versus  $l_3$  for  $\beta = 0.2$ ,  $l_1 = 1.0$ ,  $l_2 = 0.8$ ,  $d_2 = 0.0$ ,  $d_3 = 0.0$ ,  $h_2 = 2.0$  and  $h_3 = 3.0$  (Case II).

in Fig. 12 and Fig. 13. However, the stress intensity factors at the tips of crack 2 decrease with the increase of  $h_1/l_1$  for  $h_1/l_1 < 1.0$ . This was also caused by the coupling properties of the crack shielding effects and the graded property of materials.

(x) As shown in Fig. 14 and Fig. 15, the stress intensity factor at the tips of crack 1 and crack 2 decreases rapidly with the increase of  $l_3/l_1$ . This phenomena may be caused interaction of the parallel cracks. It also means that increasing of the length of crack also plays a similar role as decreasing of the distance between the two parallel cracks for the present problem. The stress intensity factors at the tips of crack 3 first increase with the increase of its length, and then they

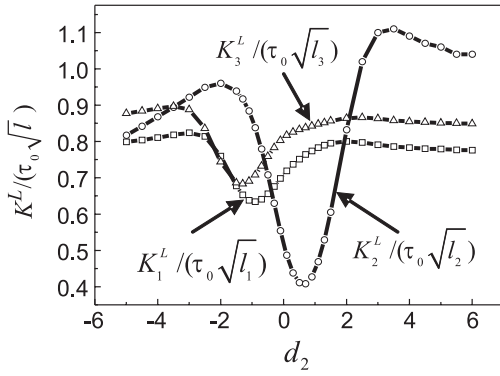


FIG. 16. Stress intensity factors at the left tips of cracks versus  $d_2$  for  $\beta = 0.2$ ,  $l_1 = 1.0$ ,  $l_2 = 1.0$ ,  $l_3 = 1.5$ ,  $d_3 = 0.0$ ,  $h_2 = 1.0$  and  $h_3 = 2.0$  (Case II).

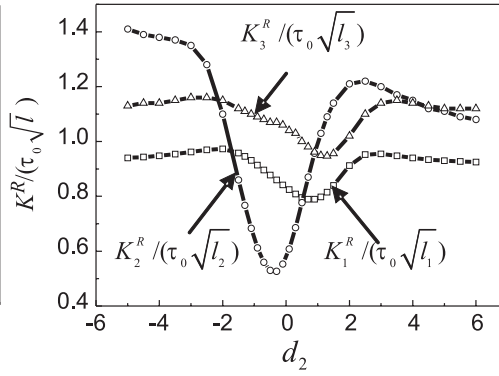


FIG. 17. Stress intensity factors at the right tips of cracks versus  $d_2$  for  $\beta = 0.2$ ,  $l_1 = 1.0$ ,  $l_2 = 1.0$ ,  $l_3 = 1.5$ ,  $d_3 = 0.0$ ,  $h_2 = 1.0$  and  $h_3 = 2.0$  (Case II).

all decrease with the increase of its length due to the large difference of material properties at both sides of the crack tips. This phenomenon was caused by the crack shielding effects.

(xi) The stress intensity factors of crack 1 and crack 3 will tend to constants for  $|d_2/l_1| > 4.0$ , as shown in Figs. 16, 17. This means that the effects of  $d_2/l_1$  on the stress intensity factors of crack 1 and crack 3 will become mild for  $|d_2/l_1| > 4.0$ . The stress intensity factors of crack 1 and crack 3 oscillate with the variation of  $d_2/l_1$  for  $|d_2/l_1| < 4.0$ , as shown in Figs. 16, 17. The stress intensity factor at the left tip of crack 2 increases oscillatory with the variation of  $d_2/l_1$ , to reach the maximum value at  $d_2/l_1 = 3.5$ , then it decreases with the increase of  $d_2/l_1$  for  $d_2/l_1 > 4.0$ , as shown in Fig. 16. The stress intensity factor at the right tip of crack 2 decreases oscillatory with the increase of  $d_2/l_1$  for  $d_2/l_1 < 2.0$  as shown in Fig. 17. So it can be concluded that the crack positions also play a very important role in the stress intensity factors of all the three parallel cracks.

(xii) As shown in Fig. 18, the stress intensity factors of crack 1 increase with the increasing of  $\beta l_1$ , to reach two different maximum values at  $\beta l_1 = -0.6$  and  $\beta l_1 = 0.6$ , respectively, then they all decrease with increasing of  $\beta l_1$ . The plots of the stress intensity factors of crack 1 are almost symmetric to each other about the line of  $\beta l_1 = 0$  for  $|\beta l_1| < 1.0$ . However, the plots of the stress intensity factors of crack 1 are not symmetric to each other about the line of  $\beta l_1 = 0$  for  $|\beta l_1| > 1.0$ . This was caused by the non-symmetric property of crack 3. As shown in Fig. 19, the stress intensity factor at the left tip of crack 2 increases rapidly with increasing of  $\beta l_1$ , to reach the maximum value at  $\beta l_1 = -0.4$ , then it decreases with the increasing of  $\beta l_1$ . The stress intensity factor at the right tip of crack 2 increases with increasing of  $\beta l_1$ , to reach the maximum value at

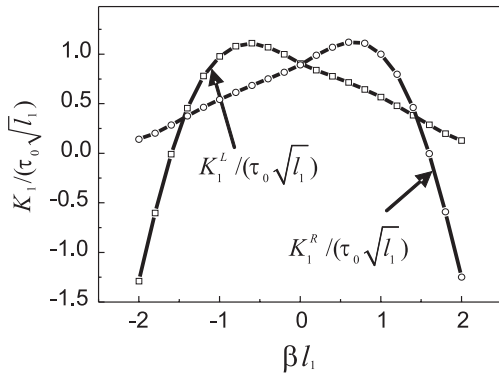


FIG. 18. Stress intensity factors at the tips of crack 1 versus  $\beta l_1$  for  $l_2/l_1 = l_3/l_1 = 1.0$ ,  $d_2/l_1 = 0.0$ ,  $d_3/l_1 = 1.0$ ,  $h_2/l_1 = 2.0$  and  $h_3/l_1 = 3.0$  (Case II).

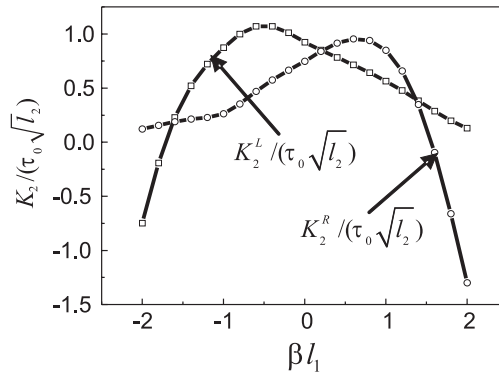


FIG. 19. Stress intensity factors at the tips of crack 2 versus  $\beta l_1$  for  $l_2/l_1 = l_3/l_1 = 1.0$ ,  $d_2/l_1 = 0.0$ ,  $d_3/l_1 = 1.0$ ,  $h_2/l_1 = 2.0$  and  $h_3/l_1 = 3.0$  (Case II).

$\beta l_1 = 0.6$ , then it decreases with increasing  $\beta l_1$ . As shown in Fig. 20, the stress intensity factors of crack 3 increase with the increasing of  $\beta l_1$ , to reach two different peak values  $K_3^L / (\tau_0 \sqrt{l_3}) = 3.17$  and  $K_3^R / (\tau_0 \sqrt{l_3}) = 1.06$  at  $\beta l_1 = -1.8$  and  $\beta l_1 = 1.4$ , respectively, then they all decrease with increasing  $\beta l_1$ . As shown in Figs. 18–20, the stress intensity factor at the left-hand tip of crack 3 is not equal to one at the right-hand tip of crack 3 for  $\beta l_1 = 0$ , because the geometric position of crack 3 is non-symmetrical. And the stress intensity factor at the left tip of crack 2 is also not equal to one at the right tip of crack 2 for  $\beta l_1 = 0$  due to the influence of non-symmetrical crack 3. However, the stress intensity factor at the left tip of crack 1 is equal to one at the right tip of crack 1 for  $\beta l_1 = 0$  due to smaller influence of non-symmetrical crack 3. This means that

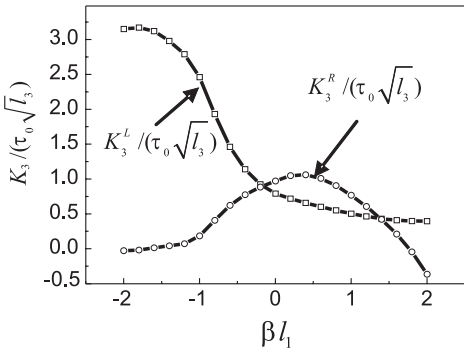


FIG. 20. Stress intensity factors at the tips of crack 3 versus  $\beta l_1$  for  $l_2/l_1 = l_3/l_1 = 1.0$ ,  $d_2/l_1 = 0.0$ ,  $d_3/l_1 = 1.0$ ,  $h_2/l_1 = 2.0$  and  $h_3/l_1 = 3.0$  (Case II).

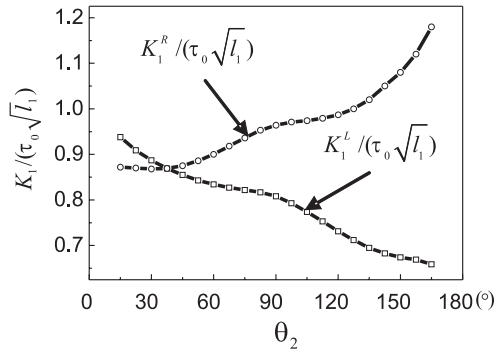


FIG. 21. Stress intensity factors at the tips of crack 1 versus  $\theta_2$  for  $\beta l_1 = 0.2$ ,  $l_2/l_1 = l_3/l_1 = 1.0$ ,  $\rho_2/l_1 = 1.5$ ,  $\rho_3/l_1 = 2.0$  and  $\theta_3 = 90^\circ$  (Case II).

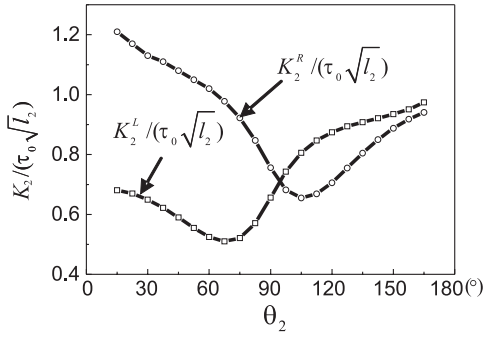


FIG. 22. Stress intensity factors at the tips of crack 2 versus  $\theta_2$  for  $\beta l_1 = 0.2$ ,  $l_2/l_1 = l_3/l_1 = 1.0$ ,  $\rho_2/l_1 = 1.5$ ,  $\rho_3/l_1 = 2.0$  and  $\theta_3 = 90^\circ$  (Case II).

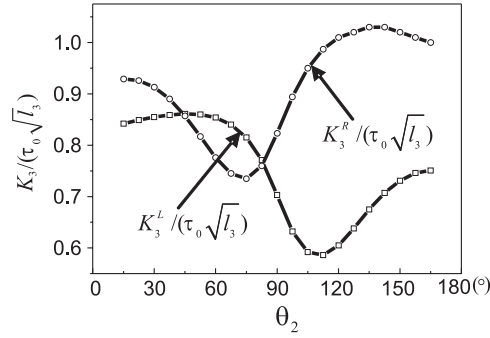


FIG. 23. Stress intensity factors at the tips of crack 3 versus  $\theta_2$  for  $\beta l_1 = 0.2$ ,  $l_2/l_1 = l_3/l_1 = 1.0$ ,  $\rho_2/l_1 = 1.5$ ,  $\rho_3/l_1 = 2.0$  and  $\theta_3 = 90^\circ$  (Case II).

the graded properties of materials also plays an important role on the intensity factors of cracks as discussed in [39].

(xiii) As shown in Figs. 21–23, the stress intensity factor at the left tip of crack 1 decrease with the increase of  $\theta_2$ . However, the intensity factor at the right tip of crack 1 increase with the increase of  $\theta_2$ . The stress intensity factors at the tips of crack 2 decrease with the increase of  $\theta_2$  until they reach the minimum values at the position of around  $\theta_2 = 67.5^\circ$  and  $\theta_2 = 105^\circ$ , respectively. Then they increase with the increase of  $\theta_2$ . The stress intensity factor at the left tip of crack 3 experiences increasing, decreasing and increasing with the increase of  $\theta_2$ , and reach the maximum value and the minimum value at ca  $\theta_2 = 45^\circ$  and  $\theta_2 = 112.5^\circ$ , respectively. The stress intensity factor at the right tip of crack 3 experiences decreasing, increasing and decreasing with the increase of  $\theta_2$ , and reach the minimum value and the maximum value at about  $\theta_2 = 75^\circ$  and  $\theta_2 = 135^\circ$ , respectively. These phenomena were also caused by the competition between the shielding effect and the graded property of materials.

## Appendix

Equation (17) can be rewritten as follows:

$$(A-1) \quad \sum_{n=0}^{\infty} a_{1n} A_n^{(13)}(x) + \sum_{n=0}^{\infty} a_{2n} B_n^{(13)}(x) + \sum_{n=0}^{\infty} a_{3n} C_n^{(13)}(x) = U^{(13)}(x),$$

$$x_1 \leq x \leq x_2,$$

$$(A-2) \quad \sum_{n=0}^{\infty} a_{1n} A_n^{(23)}(x) + \sum_{n=0}^{\infty} a_{2n} B_n^{(23)}(x) + \sum_{n=0}^{\infty} a_{3n} C_n^{(23)}(x) = U^{(23)}(x),$$

$$x_3 \leq x \leq x_4,$$

$$(A-3) \quad \sum_{n=0}^{\infty} a_{1n} A_n^{(33)}(x) + \sum_{n=0}^{\infty} a_{2n} B_n^{(33)}(x) + \sum_{n=0}^{\infty} a_{3n} C_n^{(33)}(x) = U^{(33)}(x),$$

$x_5 \leq x \leq x_6,$

where  $A_n^{(i3)}(x)$ ,  $B_n^{(i3)}(x)$ ,  $C_n^{(i3)}(x)$  and  $U^{(i3)}(x)$  ( $i = 1, 2, 3$ ) are known functions.

From Eq. (A-3) it follows:

$$(A-4) \quad \sum_{n=0}^{\infty} a_{3n} C_n^{(33)}(x) = U^{(33)}(x) - \sum_{n=0}^{\infty} a_{1n} A_n^{(33)}(x) - \sum_{n=0}^{\infty} a_{2n} B_n^{(33)}(x).$$

It can now be solved for coefficients  $a_{3n}$  by the Schmidt method. Here the form

$$U^{(33)}(x) - \sum_{n=0}^{\infty} a_{1n} A_n^{(33)}(x) - \sum_{n=0}^{\infty} a_{2n} B_n^{(33)}(x)$$

can be considered as a temporarily known function. We have

$$(A-5) \quad a_{3n} = \sum_{i=0}^{\infty} a_{1i} \beta_{ni}^{(13)} + \sum_{i=0}^{\infty} a_{2i} \beta_{ni}^{(23)} + \beta_n^{(33)},$$

with

$$\left\{ \begin{aligned} \beta_{ni}^{(13)} &= - \sum_{j=n}^{\infty} \frac{M_{nj}^{(3)}}{M_{jj}^{(3)} N_j^{(3)}} \int_{x_5}^{x_6} A_i^{(33)}(x) B_j^{(3)}(x) dx, \\ \beta_{ni}^{(23)} &= - \sum_{j=n}^{\infty} \frac{M_{nj}^{(3)}}{M_{jj}^{(3)} N_j^{(3)}} \int_{x_5}^{x_6} B_i^{(33)}(x) B_j^{(3)}(x) dx, \\ \beta_n^{(33)} &= \sum_{j=n}^{\infty} \frac{M_{nj}^{(3)}}{M_{jj}^{(3)} N_j^{(3)}} \int_{x_5}^{x_6} U^{(33)}(x) B_j^{(3)}(x) dx, \end{aligned} \right.$$

where  $M_{ij}^{(3)}$  is the cofactor of the element  $d_{ij}^{(3)}$  of matrix  $D_n^{(3)}$ , which is defined as follows:

$$(A-6) \quad D_n^{(3)} = \begin{bmatrix} d_{00}^{(3)} & d_{01}^{(3)} & d_{02}^{(3)} & \cdot & d_{0n}^{(3)} \\ d_{10}^{(3)} & d_{11}^{(3)} & d_{12}^{(3)} & \cdot & d_{1n}^{(3)} \\ d_{20}^{(3)} & d_{21}^{(3)} & d_{22}^{(3)} & \cdot & d_{2n}^{(3)} \\ \cdot & \cdot & \cdot & \cdot & \cdot \\ d_{n0}^{(3)} & d_{n1}^{(3)} & d_{n2}^{(3)} & \cdot & d_{nn}^{(3)} \end{bmatrix}, \quad d_{ij}^{(3)} = \int_{x_5}^{x_6} C_i^{(33)}(x) C_j^{(33)}(x) dx$$

and  $N_j^{(3)}$  can be constructed by a set of functions  $B_j^{(3)}(x)$ , which satisfy the orthogonality conditions as follows:

$$(A-7) \quad \int_{x_5}^{x_6} B_i^{(3)}(x)B_j^{(3)}(x)dx = N_j^{(3)}\delta_{ij}, \quad \int_{x_5}^{x_6} [B_j^{(3)}(x)]^2 dx = N_j^{(3)}$$

and  $B_j^{(3)}(x)$  can be constructed from the function  $C_i^{(33)}(x)$ :

$$(A-8) \quad B_j^{(3)}(x) = \sum_{i=0}^j \frac{M_{ij}^{(3)}}{M_{jj}^{(3)}} C_i^{(33)}(x).$$

Substituting Eq. (A-5) into Eq. (A-1) to Eq.(A-2), respectively, we have

$$(A-9) \quad \sum_{n=0}^{\infty} a_{1n}A_n^{(3)}(x) + \sum_{n=0}^{\infty} a_{2n}B_n^{(3)}(x) = U^{(12)}(x), \quad x_1 \leq x \leq x_2,$$

$$(A-10) \quad \sum_{n=0}^{\infty} a_{1n}A_n^{(22)}(x) + \sum_{n=0}^{\infty} a_{2n}B_n^{(22)}(x) = U^{(22)}(x), \quad x_3 \leq x \leq x_4,$$

where

$$\left\{ \begin{array}{l} A_i^{(12)}(x) = A_i^{(13)}(x) + \sum_{n=0}^{\infty} \beta_{ni}^{(13)} C_n^{(13)}(x), \\ B_i^{(12)}(x) = B_i^{(13)}(x) + \sum_{n=0}^{\infty} \beta_{ni}^{(23)} C_n^{(13)}(x), \\ U^{(12)}(x) = U^{(13)}(x) - \sum_{n=0}^{\infty} \beta_n^{(33)} C_n^{(13)}(x), \end{array} \right.$$

and

$$\left\{ \begin{array}{l} A_i^{(22)}(x) = A_i^{(23)}(x) + \sum_{n=0}^{\infty} \beta_{ni}^{(13)} C_n^{(23)}(x), \\ B_i^{(22)}(x) = B_i^{(23)}(x) + \sum_{n=0}^{\infty} \beta_{ni}^{(23)} C_n^{(23)}(x), \\ U^{(22)}(x) = U^{(23)}(x) - \sum_{n=0}^{\infty} \beta_n^{(33)} C_n^{(23)}(x). \end{array} \right.$$

Repeating steps (A-4)–(A-8) for Eq. (A-10), we obtain:

$$(A-11) \quad a_{2n} = \sum_{i=0}^{\infty} a_{1i}\beta_{ni}^{(3)} + \beta_n^{(22)},$$

where  $\beta_{ni}^{(12)}$  and  $\beta_n^{(22)}$  can be derived in the same way as the above ones  $\beta_{ni}^{(13)}$ ,  $\beta_{ni}^{(23)}$  and  $\beta_n^{(33)}$ . For brevity, they were omitted in the present paper.

Substituting Eq. (A-11) into Eq. (A-9), we have

$$(A-12) \quad \sum_{n=0}^{\infty} a_{1n} A_n^{(11)}(x) = U^{(11)}(x), \quad x_1 \leq x \leq x_2,$$

where

$$\begin{cases} A_i^{(11)}(x) = A_i^{(12)}(x) + \sum_{n=0}^{\infty} \beta_{ni}^{(12)} B_n^{(12)}(x), \\ U^{(11)}(x) = U^{(12)}(x) - \sum_{n=0}^{\infty} \beta_n^{(22)} B_n^{(12)}(x). \end{cases}$$

Repeating steps (A-4)–(A-8) for Eq. (A-12), the unknown coefficients  $a_{1n}$  can be obtained as follows:

$$(A-14) \quad a_{1n} = \beta_n^{(11)},$$

where  $\beta_n^{(11)}$  can be derived in the same way as the above one concerning  $\beta_n^{(33)}$ . For brevity, they have been omitted in the present paper.

With the aid of Eqs. (A-14), (A-11) and (A-5), the unknown coefficients  $a_{1n}$ ,  $a_{2n}$  and  $a_{3n}$  can be obtained.

## Acknowledgments

This work was financially supported by the National Natural Science Foundation of China (90405016).

## References

1. H.G. BEOM, S.N. ATLURI, *Near-tip fields and intensity factors for interfacial cracks in dissimilar anisotropic piezoelectric media*, International Journal of Fracture, **75**, 163–183, 1996.
2. H. GAO, T.Y. ZHANG, P. TONG, *Local and global energy rates for an elastically yielded crack in piezoelectric ceramics*, Journal of Mechanics and Physics of Solids, **45**, 491–510, 1997.
3. XUE-LI HAN, TZUCHIANG WANG, *Interacting multiple cracks in piezoelectric materials*, International Journal of Solids and Structures, **36**, 4183–4202, 1999..
4. K. NARITA, Y. SHINDO, K. WATANABE, *Anti-plane shear crack in a piezoelectric layered to dissimilar half-spaces*, JSME International Journal, Ser. A, **42**, 66–72, 1999.
5. S.W. YU, Z.T. CHEN, *Transient response of a cracked infinite piezoelectric strip under anti-plane impact*, Fatigue of Engineering Materials and Structures, **21**, 1381–1388, 1998.

6. T.Y. ZHANG, J.E. HACK, *Mode-III cracks in piezoelectric materials*, Journal of Applied Physics, **71**, 5865–5870, 1992.
7. K. TAKAGI, J.F. LI, S. YOKOYAMA, R. WATANABE, *Fabrication and evaluation of PZT/Pt piezoelectric composites and functionally graded actuators*, Journal of the European Ceramic Society, **10**, 1577–1583, 2003.
8. D.R. JIN, *Functionally graded PZT/ZnO piezoelectric composites*, Journal of Materials Science Letters, **22**, 971–974, 2003.
9. G.J. WENG, C.Y. LI, *Anti-plane crack problem in functionally graded piezoelectric materials*, Journal of Applied Mechanics, **69**, No. 4, 481–488, 2002.
10. S. UEDA, *Transient response of a center crack in a functionally graded piezoelectric strip under electromechanical impact*, Engineering Fracture Mechanics, **73**, 1455–1471, 2006.
11. J. CHEN, Z.X. LIU, Z.Z. ZOU, *Electriomechanical impact of a crack in a functionally graded piezoelectric medium*, Theoretical and Applied Fracture Mechanics, **39**, 47–60, 2003.
12. B. JIN, Z. ZHONG, *A moving mode-III crack in functionally graded piezoelectric material: permeable problem*, Mechanics Research Communications, **29**, 217–224, 2002.
13. B.L. WANG, *A mode-III crack in functionally graded piezoelectric materials*, Mechanics Research Communications, **30**, 151–159, 2003.
14. SOON MAN KWON, *Electrical nonlinear anti-plane shear crack in a functionally graded piezoelectric strip*, International Journal of Solids and Structures, **40**, 5649–5667, 2003.
15. L.Y. JIANG, *The fracture behavior of functionally graded piezoelectric materials with dielectric cracks*, International Journal of Fracture, **149**, 87–104, 2008.
16. Z.G. ZHOU, Z.T. CHEN, *Basic solution of a Mode-I limited-permeable crack in functionally graded piezoelectric/piezomagnetic materials*, International Journal of Solids and Structures, **45**, No. 7-8, 2265–2296, 2008.
17. J. SLADEK, V. SLADEK, C.H. ZHANG, P. SOLEK, E. PAN, *Evaluation of fracture parameters in continuously nonhomogeneous piezoelectric solids*, International Journal of Fracture, **145**, 313–326, 2007.
18. B.N. RAO, M. KUNA, *Interaction integrals for fracture analysis of functionally graded piezoelectric materials*, International Journal of Solids and Structures, **45**, 5237–5257, 2008.
19. Z.G. ZHOU, B. WANG, *The behavior of two parallel symmetry permeable interface cracks in a piezoelectric layer bonded to two half piezoelectric materials planes*, International Journal of Solids and Structures, **39**, 17, 4485–4500, 2002.
20. Z.G. ZHOU, B. WANG, *The behavior of two parallel symmetric permeable cracks in piezoelectric materials*, Applied Mathematics and Mechanics, **23**, 1357–1366, 2002.
21. Z.G. ZHOU, S.Y. DU, B. WANG, *Dynamic behavior of two parallel symmetric permeable cracks in a piezoelectric material strip*, Acta Mechanica Solida Sinica, **15**, 1, 294–302, 2002.
22. J.L. SUN, Z.G. ZHOU, B. WANG, *Dynamic behavior of two unequal parallel permeable interface cracks in a piezoelectric layer bonded to two half piezoelectric materials planes*, Applied Mathematics and Mechanics, **26**, 2, 160–170, 2005.
23. J.L. SUN, Z.G. ZHOU, B. WANG, *Dynamic behavior of unequal parallel permeable interface multi-cracks in a piezoelectric layer bonded to two piezoelectric materials half-planes*, European Journal of Mechanics and Solids, **23**, 6, 993–1005, 2004.

24. Z.G. ZHOU, B. WANG, *Two parallel symmetric permeable cracks in functionally graded piezoelectric/piezomagnetic materials under anti-plane shear loading*, International Journal of Solids and Structures, **41**, 4407–4422, 2004.
25. Z.H. TONG, C.P. JIANG, S.H. LO, Y.K. CHEUNG, *A closed form solution to the antiplane problem of doubly periodic cracks of unequal size in piezoelectric materials*, Mechanics of Materials, **38**, 269–286, 2006.
26. J. CHEN, Z.X. LIU, *On the dynamic behavior of a functionally graded piezoelectric strip with periodic cracks vertical to the boundary*, International Journal of Solids and Structures, **42**, 3133–3146, 2005.
27. B.L. WANG, J.C. HAN, *Multiple surface cracks in a piezoelectric layer bonded to an elastic substrate under transient electromechanical loads*, Mechanics of Materials, **39**, 291–304, 2007.
28. J.J. HAN, Y.H. CHEN, *Multiple parallel cracks interaction problem in piezoelectric ceramics*, International Journal of Solids and Structures, **36**, 3375–3390, 1999.
29. P.M. MORSE, H. FESHBACH, *Methods of Theoretical Physics*, McGraw-Hill, New York, **1**, 828–930, 1958.
30. A.K. SOH, D.N. FANG, K.L. LEE, *Analysis of a bi-piezoelectric ceramic layer with an interfacial crack subjected to anti-plane shear and in-plane electric loading*, European Journal of Mechanics. A/Solid, **19**, 6, 961–977, 2000.
31. F. DELALE, F. ERDOGAN, *On the mechanical modeling of the interfacial region in bonded half-planes*, ASME Journal of Applied Mechanics, **55**, 317–324, 1988.
32. H. FILDIS, O.S. YAHSI, *The axisymmetric crack problem in a non-homogeneous interfacial region between homogeneous half-spaces*, International Journal of Fracture, **78**, 139–163, 1996.
33. L.C. GUO, N. NODA, *Modeling method for a crack problem of functionally graded materials with arbitrary properties—piecewise-exponential model*, International Journal of Solids and Structures, **44**, 6768–6790, 2007.
34. I.S. GRADSHTEYN, I.M. RYZHIK, *Table of Integral, Series and Products*, Academic Press, New York, 1035–1037, 1980.
35. A. ERDELYI, *Tables of Integral Transforms*, Vol. 1, McGraw-Hill, New York. 34–89, 1954.
36. S. ITOU, *Three dimensional waves propagation in a cracked elastic solid*, Journal of Applied Mechanics, **45**, 5, 807–811, 1978.
37. Z.G. ZHOU, Y.Y. BAI, X.W. ZHANG, *Two collinear Griffith cracks subjected to uniform tension in infinitely long strip*, International Journal of Solids and Structures, **36**, 36, 5597–5609, 1999.
38. M. RATWANI, G.D. GUPTA, *Interaction between parallel cracks in layered composites*, International Journal of Solids and Structures, **10**, 7, 701–708, 1974.
39. N.I. SHBEEB, W.K. BINIENDA, *Analysis of an interface crack for a functionally graded strip sandwiched between two homogeneous layers of finite thickness*, Engineering Fracture Mechanics, **64** 3, 693–720, 1999.

Received October 15, 2008; revised version March 16, 2009.

---